Universal feature in optical control of a *p*-wave Feshbach resonance

Peng Peng,[1,2] Ren Zhang,[3,4] Lianghui Huang,[1,2,*] Donghao Li,[1,2] Zengming Meng,[1,2] Pengjun Wang,[1,2] Hui Zhai,[4,5] Peng Zhang,[6,7] and Jing Zhang[1,8,†]

[1]*State Key Laboratory of Quantum Optics and Quantum Optics Devices, Institute of Opto-Electronics, Shanxi University, Taiyuan 030006, People's Republic of China*

[2]*Collaborative Innovation Center of Extreme Optics, Shanxi University, Taiyuan 030006, People's Republic of China*

[3]*School of Science, Xi'an Jiaotong University, Shanxi 710049, China*

[4]*Institute for Advanced Study, Tsinghua University, Beijing 100084, China*

[5]*Collaborative Innovation Center of Quantum Matter, Beijing 100084, China*

[6]*Department of Physics, Renmin University of China, Beijing 100872, China*

[7]*Beijing Computational Science Research Center, Beijing 100084, China*

[8]*Synergetic Innovation Center of Quantum Information and Quantum Physics, University of Science and Technology of China, Hefei, Anhui 230026, People's Republic of China*

(Received 27 October 2017; published 10 January 2018)

We report the experimental results on the optical control of a *p*-wave Feshbach resonance by utilizing a laser-driven bound-to-bound transition to shift the energy of a closed-channel molecule state. The magnetic field location for the *p*-wave resonance as a function of laser detuning can be captured by a simple formula with essentially one parameter, which describes how sensitively the resonance depends on the laser detuning. The key result of this work is to demonstrate, both experimentally and theoretically, that the ratio between this parameter for the $m = 0$ component of the resonance and that for the $m = \pm 1$ component, to a large extent, is universal. We also show that this optical control can create intriguing situations where interesting few- and many-body physics can occur, such as a *p*-wave resonance overlapping with an *s*-wave resonance or the three components of a *p*-wave resonance being degenerate.

DOI: 10.1103/PhysRevA.97.012702

I. INTRODUCTION

The capability to control the interaction strength between atoms has led to tremendous progress in the field of ultracold-atomic gases. Magnetic-field-induced Feshbach resonance is one of such powerful tools and has been widely used in studying strongly correlated degenerate atomic gases [1]. Another technique for tuning interatomic interactions is the optical Feshbach resonance, in which a pair of atoms in the scattering states is coupled to an excited molecular state by a near photoassociation resonance laser field [2]. The optical Feshbach resonance offers a more flexible spatial and temporal control of interaction since the laser intensity can vary on short-length and -time scales [3,4]. However, it also suffers from rapid losses of atoms due to the light-induced inelastic collisions between atoms.

Recently, an alternative method of optical control has been implemented to avoid the problem of atom losses, in which the optical control is combined with the magnetic Feshbach resonance [5–14]. The key idea is that instead of coupling atoms in scattering states to a bound state, the laser induces a bound-to-bound transition between the closed-channel molecule responsible for a magnetic Feshbach resonance and an excited molecular state. In this way, the laser can shift the energy of the closed-channel molecule, and thus moves the location of the magnetic Feshbach resonance. This method has been recently demonstrated in both ultracold Bose [6,8,11] and Fermi [10,12] gases. It has been shown that the atom-loss rate can be reduced by an order of magnitude, while the advantage of high resolution of spatial and temporal control is still maintained. To distinguish this method from the conventional optical Feshbach resonance, we shall refer to it as the optical control of a magnetic Feshbach resonance.

The *p*-wave interaction plays a crucial role in many quantum many-body systems [15–21], especially in the realization of topological superfluids [22–24]. Thus, intensive experimental efforts have been made on *p*-wave Feshbach resonance in the last decade [25–33]. In this paper, we apply the method of optical control to a higher partial-wave magnetic Feshbach resonance. We will highlight the universal features in such an optical control. In addition, we will show that interesting situations such as degenerate *p*-wave and *s*- and *p*-wave overlapping resonances can indeed be created.

This paper is arranged as follows: In Sec. II, we describe our experimental setup and show the bound-to-bound spectroscopy for excited $^{40}K_2$ molecules, which is used as a frequency calibration in our further experiments. In Sec. III, we show the shift of *p*-wave resonance, which is induced by a laser beam polarized along the direction of the magnetic field (i.e., the π-polarized light). In this section, we focus on the universal feature of such optical shift. Section IV is devoted to the theoretical explanation of that universal feature. The

*huanglh06@126.com

†jzhang74@yahoo.com, jzhang74@sxu.edu.cn

laser-induced overlapping of s- and p-wave resonance is illustrated in Sec. V. In Sec. IV, we show the shift induced by the laser with polarization perpendicular to the magnetic field (i.e., the σ-polarized light). Some discussions are given in Sec. VII. In the Appendix, we show some detail of our theoretical analysis.

II. EXPERIMENTAL SETUP

Our experiment is performed with a ^{40}K Fermi gas in the $F = 9/2$ manifold with atom number $N = 2 \times 10^6$ and at temperature $T/T_F \approx 0.3$ in a crossed 1064 nm optical dipole trap. Here, T_F is the Fermi temperature defined as $T_F = (6N)^{1/3}\hbar\bar{\omega}/k_B$, with $\bar{\omega} \simeq 2\pi \times 80$ Hz labeling the geometric trapping frequency. The fermionic atoms are transferred to the $|9/2, -9/2\rangle$ state as the initial state via a rapid adiabatic passage induced by a radio frequency (rf) field at 5 G. Then, the Fermi gas is transferred to the $|9/2, -7/2\rangle$ state using a rf field with duration of 30 ms at $B \simeq 219.4$ G, where the frequency of center is 47.45 MHz and the width is 0.3 MHz. In addition, we can also prepare the Fermi gases at the $|9/2, -5/2\rangle$ state via transferring atoms in the $|9/2, -7/2\rangle$ state to the $|9/2, -5/2\rangle$ state by a rf field of π pulse.

Subsequently, a homogeneous magnetic bias field $B_{\rm exp}$ produced by quadrupole coils is applied in the $\hat{z}$ axis (gravity direction). The laser beam propagating along $\hat{y}$ or $\hat{z}$, respectively, is used as the tool to manipulate the p-wave Feshbach resonance. The laser beam is extracted from a continuous-wave Ti-sapphire single-frequency laser and focused at the position of the atomic cloud with $1/e^2$ radii of 200 μm, which is larger than the size of the degenerate Fermi gas. The laser beams are frequency shifted by an acousto-optic modulators (AOM), which allows precise control of the laser intensity and duration of the pulse.

In order to observe and control the p-wave Feshbach resonance, we start with the ultracold Fermi gases in the $|9/2, -7/2\rangle$ state at $B \simeq 219.4$ G. Then we adiabatically ramp the magnetic field to the various expected field $B_{\rm exp}$ in 1 ms, and hold 20 ms to observe the atomic losses at the $|9/2, -7/2\rangle$ state by counting the number of atoms. Then the laser is switched on and couples the closed-channel molecular state to the excited molecular states, as shown in Fig. 1(a). Finally, we immediately turn off the laser beams, the optical trap, and the magnetic field, and let the atoms ballistically expand in 12 ms and take the time-of-flight (TOF) absorption image. The number of atoms in the $|9/2, -7/2\rangle$ state is obtained from the TOF image.

To calibrate the experimental setup, we first measure the bound-to-bound spectroscopy for excited $^{40}K_2$ molecules below the $^2P_{1/2} + {}^2S_{1/2}$ threshold near p-wave Feshbach resonance. The magnetic field $B_{\rm exp}$ is set to be 198.3 G. At this value, the atoms are subject to inelastic loss since the energy of the closed-channel molecular state $m = \pm 1$ coincides with the energy of two free atoms. When the laser illuminates the atomic gas and is near resonant with a bound-to-bound transition from ϕ_g to one of the excited molecular states ϕ_e, shift of the resonance position is induced by the ac-Stark effect, exhibiting displacement of the peak of atomic loss spectroscopy. Figure 1(b) shows the bound-to-bound spectroscopy near p-wave Feshbach resonance. Here, the laser intensity is

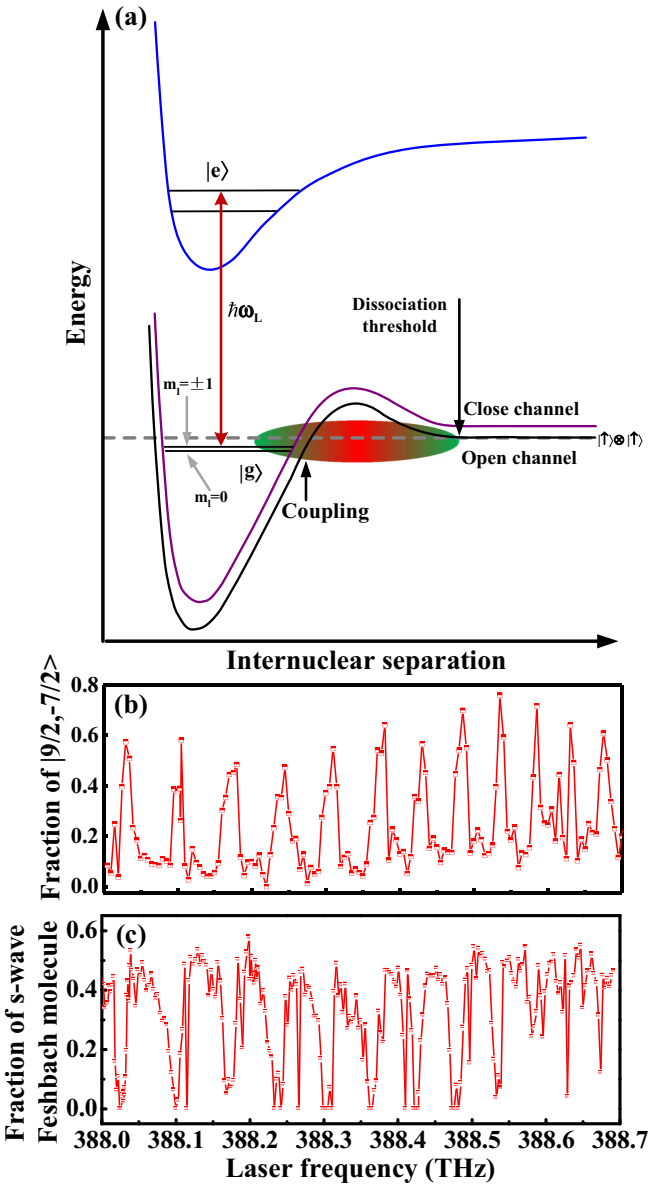

FIG. 1. Energy-level diagram and excited molecule state spectroscopy. (a) Schematic diagram of the energy curves of two atoms. A bound-to-bound transition from closed-channel molecular state ϕ_g to one of the excited molecular states ϕ_e occurs when a near-resonant laser with frequency ω_L is applied. Two curves at the low-energy end denote the energy of two single-component ^{40}K atoms in the electronic ground state. The curve at the high-energy end denotes the energy of two atoms composed of one electronic ground-state atom and one electronic excited state atom. (b) Bound-to-bound spectroscopy below the $^2P_{1/2} + {}^2S_{1/2}$ threshold near p-wave Feshbach resonance of $|9/2, -7/2\rangle \otimes |9/2, -7/2\rangle$ at the magnetic field $B = 198.3$ G. (c) Bound-to-bound spectroscopy below the $^2P_{1/2} + {}^2S_{1/2}$ threshold near s-wave Feshbach resonance of $|9/2, -9/2\rangle \otimes |9/2, -7/2\rangle$ at the magnetic field $B = 202.1$ G.

$I = 60$ mW and the laser wavelength ranges from 771.5 to 772.7 nm.

We compare this bound-to-bound spectroscopy near p-wave Feshbach resonance with that near s-wave Feshbach resonance of $|9/2, -9/2\rangle \otimes |9/2, -7/2\rangle$ at the magnetic

field $B = 202.1$ G, shown in Fig. 1(c), which was reported in our earlier work [10]. In Ref. [10], Feshbach molecules are prepared in the BEC regime of the resonance at $B = 202.1$ G and the atomic loss spectroscopy is measured during the laser drive of the bound-to-bound transition. The bound-to-bound spectroscopy obtained by these two different ways shows a high level of consistency. The observed peaks in the bound-to-bound spectroscopy near p-wave Feshbach resonance correspond to the vibrational level of the excited molecular states. There should be the multisubstructures at each vibrational level induced by vibration, rotation, hyperfine interaction, and Zeeman interaction of molecules, which were observed in the bound-to-bound spectroscopy near s-wave Feshbach resonance in Ref. [10].

In addition, in this work we focus on the influence of the laser beam on the magnetic Feshbach resonance point. In our system, there are two main loss mechanisms, i.e., the three-body loss induced by the three-body recombination process, and the two-body loss induced by the spontaneous emission of the excited molecule states. Both of the loss effects are significantly enhanced when the resonance occurs. Thus, in our experiments, we measure the total atom loss as a function of magnetic field and identify the magnetic field with maximum loss to be the resonance point.

III. OPTICAL SHIFT OF RESONANCE POSITION AND THE UNIVERSAL FEATURE

We start with the p-wave resonance for two atoms in $|9/2, -7/2\rangle \otimes |9/2, -7/2\rangle$ with a magnetic field along the $\hat{z}$ direction. Because of the magnetic dipolar interaction, the $m = 0$ resonance occurs at a slightly higher field of 198.8 G and the $m = \pm 1$ resonance at a slightly lower field of 198.3 G, as shown in Figs. 2(b1) and 2(c1). We first consider the situation that a laser with linear polarization along $\hat{z}$ (i.e., the π-polarized light) is applied to the sample, as shown in Fig. 2(a). Both the rotational and the time-reversal symmetry are still preserved, under the condition that the photon recoil energy is sufficiently weak compared to the detuning and can be safely ignored. Hence, the $m = \pm 1$ resonances remain degenerate even in the presence of the optical control laser.

When the laser is red detuned to the bound-to-bound transition, the energy of the closed-channel bound state is effectively pushed down due to the coupling to the excited molecular state. For the p-wave Feshbach resonance of $|9/2, -7/2\rangle \otimes |9/2, -7/2\rangle$, the magnetic momentum of the closed channel is larger than that of the open channel. Consequently, it requires larger Zeeman energy to bring the bound state to threshold, and the Feshbach resonance moves toward high magnetic fields. When the laser detuning becomes smaller, the bound-state energy experiences stronger level repulsion. As a result, the shift of the resonance position becomes larger. As shown in Fig. 2(c), we find that the position of the $m = 0$ resonance moves much faster than those of the $m = \pm 1$ resonances as the detuning decreases. For instance, when the red detuning is $\sim$1.55 GHz, as shown in Fig. 2(c4), the $m = \pm 1$ resonance is only shifted to 198.8 G and the $m = 0$ resonance is shifted to 201.6 G.

When the laser is blue detuned, the energy of the closed-channel molecule is effectively pushed to higher energy, and it therefore requires less Zeeman energy to bring the molecule to threshold, and consequently the Feshbach resonances move toward lower magnetic fields. Similarly, the resonance of $m = 0$ moves faster. Hence, for small detuning, the $m = 0$ resonance locates at a lower field than $m = 1$ resonance, as shown in Fig. 2(b4). Nevertheless, when the detuning becomes larger, it will eventually recover the situation in the absence of the laser field, that is, the $m = 0$ resonance locates at a higher field than the $m = \pm 1$ resonance, as shown in Fig. 2(b2). Hence, at a specific intermediate detuning, the $m = 0$ resonance will overlap with the $m = \pm 1$ resonance, creating another interesting situation that all three resonances appear as a single resonance. This is indeed observed, as shown in Fig. 2(b3). In other words, this happens when the difference in dipolar interaction energy between molecules is canceled by the difference in the molecular ac-Stark effect. In this specific situation, the SU(2) rotational symmetry is restored.

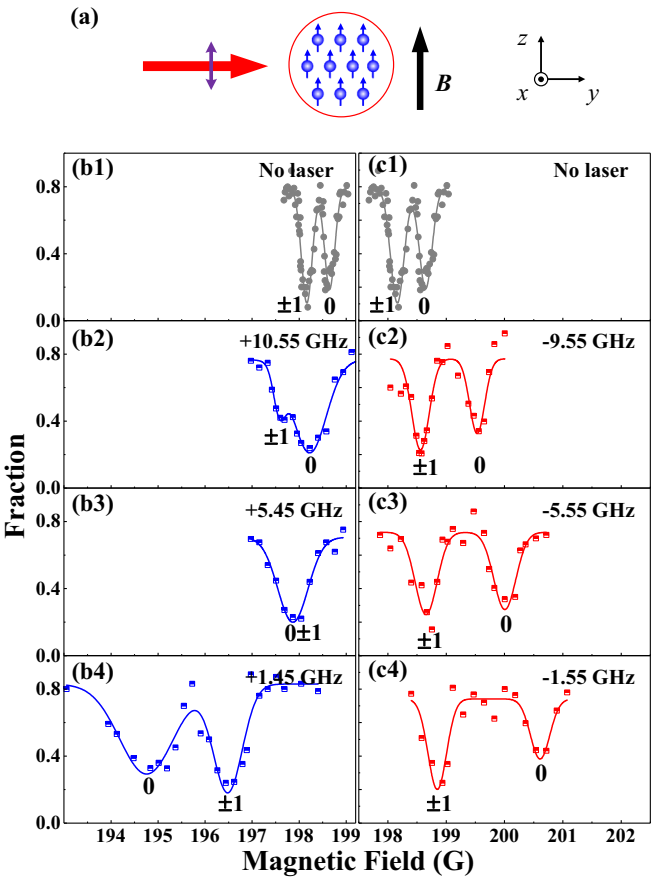

FIG. 2. The p-wave Feshbach resonance manipulated by a laser field with polarization parallel to the external magnetic field. (a) Schematic diagram of the laser beam and the external magnetic field. (b),(c) Atom-loss measurements of the p-wave Feshbach resonance of $|9/2, -7/2\rangle \otimes |9/2, -7/2\rangle$ (located at 198.3 G for $m = \pm 1$ and 198.8 G for $m = 0$ without laser field) as a function of the magnetic field for (b) blue and (c) red laser detuning. The laser field drives a bound-to-bound transition around $\omega_{eg} \simeq 388.105$ THz. The intensity of the laser is 50 mW.

To clearly visualize how the resonance position is shifted by the laser, in Fig. 3 we plot the magnetic field location as a function of the laser detuning. In Fig. 3(a), we consider the p-wave resonance for spinless ^{40}K in the $|9/2, -7/2\rangle$ state

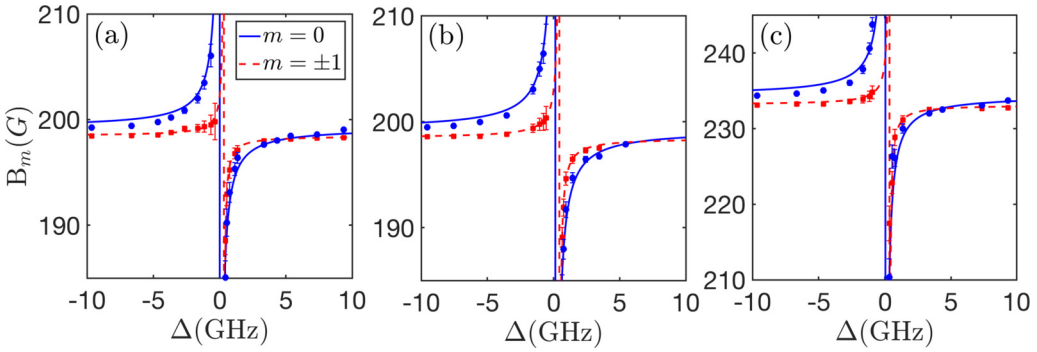

FIG. 3. The position of the shifted Feshbach resonance as a function of the laser detuning. (a),(b) p-wave Feshbach resonance of two atoms in the $|9/2,-7/2\rangle \otimes |9/2,-7/2\rangle$ state [25] at about 198 G using a bound-to-bound transition with frequency (a) $\omega_{\rm eg} \simeq 388.105$ THz and (b) $\omega_{\rm eg} \simeq 388.31$ THz. (c) p-wave Feshbach resonance of two atoms in the $|9/2,-5/2\rangle \otimes |9/2,-5/2\rangle$ state [34] at about 232 G using a bound-to-bound transition with frequency $\omega_{\rm eg} \simeq 388.105$ THz. The curves are obtained by fitting experimental data using Eq. (1).

[25] and the bound-to-bound transition at $\omega_{\rm eg} \simeq 388.105$ THz; and in Fig. 3(b), we consider the same p-wave resonance but a different bound-to-bound transition at $\omega_{\rm eg} \simeq 388.31$ THz. In Fig. 3(c), we consider a different p-wave resonance for spinless ^{40}K in the $|9/2,-5/2\rangle$ state [34] with the bound-to-bound transition at a similar frequency as Fig. 3(a).

In Fig. 3, we also show that all these cases can be well captured by the simple equation as

$$\mu(B_m - B_{m0}) = -\mathrm{Re}\left[\frac{I(m)}{\Delta - i\gamma/2}\right], \tag{1}$$

where B_m and B_{m0} are the magnetic field position for resonances in the presence and in the absence of the laser field, respectively, μ is the magnetic moment difference between the closed and open channels, Δ is the laser detuning from the excited molecular states, and γ is the spontaneous-emission rate of excited molecular states. $I(m)$ represents the laser-induced coupling between the closed-channel molecule and the excited molecular state. The right-hand side of Eq. (1) is simply the laser-induced energy shift of the closed-channel bound state. This formula can be derived from a microscopic coupled-channel model [35,36].

By fitting the data shown in Fig. 3 with Eq. (1), we find $I(0)/I(\pm 1) \approx 2.1$, 1.9, and 1.9 for Figs. 3(a)–3(c), respectively. This strongly indicates that $I(0)/I(\pm 1)$ *is a universal number*. Here, *universal* means that this ratio is not sensitive to either the choice of closed molecule, that is, which p-wave resonance to start with [e.g., Figs. 3(a) and 3(c)], or the choice of the excited molecular state, that is, which bound-to-bound transition to couple to [e.g., Figs. 3(a) and 3(b)].

IV. THEORETICAL EXPLANATION OF THE UNIVERSAL FEATURE

Here we offer a theoretical explanation of why $I(0)/I(\pm 1)$ is indeed universal. To start with, let us state the necessary quantum numbers to describe a diatomic molecular state in the center-of-mass frame. $\mathbf{r}_n$ denotes the displacement between two nuclei, and $\mathbf{r}_{e_1}$ and $\mathbf{r}_{e_2}$ are the displacements between the two electrons and the center of mass. The necessary quantum numbers include (i) the total angular momentum l and its $\hat{z}$ component m (here, $\hat{x}$, $\hat{y}$, and $\hat{z}$ label directions in the laboratory frame), (ii) the projection of $\mathbf{L}_{e_1} + \mathbf{L}_{e_2}$ along the direction of $\hat{\mathbf{r}}_n$, denoted by λ, (iii) $n_{\rm n}$ denoting the vibration between two nuclei, and a set of quantum numbers $\{n_{\rm e}\}$ describing the vibration of two electrons, and (iv) the quantum numbers describing the electron and nuclear spin degree of freedom.

For the problem considered here, it is quite reasonable to make the following assumptions: (i) The energy splitting between different spin states is much smaller compared to the laser detuning, such that we can ignore the spin-orbit coupling and the hyperfine coupling, and therefore we will not explicitly include the electron and nuclear spin degree of freedoms. (ii) The energy splittings between states with different quantum number l are also considered to be small compared to the laser detuning and, therefore, we treat them as "degenerate" states in the laser coupling. (iii) The radial wave functions of the excited molecular states are not sensitive to the quantum numbers l and m. Assumptions (ii) and (iii) are essentially based on the consideration that the molecules involved in this process are deeply bound such that their wave functions largely reside in the centrifugal barrier.

Moreover, due to the rotational symmetry along $\hat{z}$, m is a good quantum number between the initial and final states. With assumptions (i) and (ii), the laser coupling between closed and excited molecular states is proportional to

$$I(m) \propto \sum_{l^{\rm f}} \left|\left\langle l^{\rm f}, m, \lambda^{\rm f}, \{n_{\rm e}^{\rm f}\}, n_{\rm n}^{\rm f} \middle| \hat{T}_0 \middle| l^{\rm i}, m, \lambda^{\rm i}, \{n_{\rm e}^{\rm i}\}, n_{\rm n}^{\rm i} \right\rangle\right|^2, \tag{2}$$

where $\hat{T}_0$ denotes the $\hat{z}$ component of $\mathbf{r}_{e_1} + \mathbf{r}_{e_2}$, and f and i in the upper superscript label the quantum numbers for the initial- and final-state quantum numbers, respectively. Since we consider a p-wave resonance, the closed-channel molecule should be a p-wave one, that is, $l^{\rm i} = 1$; and for two alkali atoms in the electronic ground state (Σ orbital), $\lambda^{\rm i} = 0$. In the expression for $I(m)$, the different choice of $n_{\rm n}^{\rm i}$ and $\{n_{\rm e}^{\rm i}\}$ corresponds to different closed-channel molecules and, thus, different p-wave resonance; and the different choice of $n_{\rm n}^{\rm f}$ and $\{n_{\rm e}^{\rm f}\}$ corresponds to different excited-state molecules and, thus, different bound-to-bound transition frequency.

The key theoretical result is to show that $I(m)$ can be factorized into

$$I(m) = g(m, \lambda^{\rm f}) h\left(\{n_{\rm e}^{\rm f}\}, n_{\rm n}^{\rm f}, \{n_{\rm e}^{\rm i}\}, n_{\rm n}^{\rm i}, \lambda^{\rm f}\right), \tag{3}$$

where g and h are two functions. This result follows from assumption (iii) and the use of the Born adiabatic approximation. Thus, we can see that $I(0)/I(\pm1)$ only depends on λ^{f} and

$$\frac{I(0)}{I(\pm1)} = \begin{cases} 3 \text{ for } \lambda^{\mathrm{f}} = 0, \\ 1/2 \text{ for } \lambda^{\mathrm{f}} = \pm1. \end{cases} \tag{4}$$

$I(0)/I(\pm1)$ is independent of $n_{\mathrm{n}}^{\mathrm{f}}$, $\{n_{\mathrm{e}}^{\mathrm{f}}\}$, $n_{\mathrm{n}}^{\mathrm{i}}$, and $\{n_{\mathrm{e}}^{\mathrm{i}}\}$, that is to say, it is independent of the choice of p-wave resonance and, up to these two different values, it is independent of the choice of the bound-to-bound transition. The detailed proof of Eqs. (3) and (4) can be found in the Appendix.

This result provides a qualitative explanation of the experimental observations. Assuming the three cases shown in Fig. 3 all come from excited molecular states with $\lambda^{\mathrm{f}} = 0$, it is consistent with the fact that the $m = 0$ resonance always moves faster than the $m = \pm1$ resonance, and the ratio $I(0)/I(\pm1)$ is nearly a constant. The quantitative difference between our theoretical and experimental results is likely due to the assumptions (i)–(iii) being not perfectly obeyed in practice.

V. OVERLAPPING OF *s*- AND *p*-WAVE RESONANCE

Recently, several works have predicted that interesting many-body physics can occur when a p-wave Feshbach resonance sits nearby an s-wave one [37–40]. For instance, it has been predicted that for a one-dimensional Fermi gas with strong s-wave interaction, an extra p-wave interaction can make the system favor an itinerant ferromagnetic phase, providing a new mechanism for itinerant ferromagnetism [39,40]; and it has also been predicted that the interesting pairing structure can happen for a three-dimensional Fermi gas with overlapping s- and p-wave resonances [37,38]. Nevertheless, without the optical control, even in the most promising situation of ^{40}K, the p-wave resonances sitting at

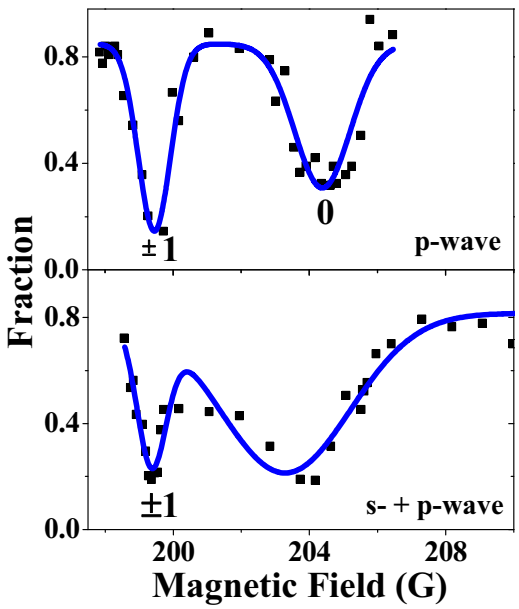

FIG. 4. Overlapping a p-wave Feshbach resonance with an s-wave resonance by applying a laser field. (a) Loss measurements of the p-wave Feshbach resonance of $|9/2,-7/2\rangle \otimes |9/2,-7/2\rangle$ as a function of the magnetic field for red laser detuning. (b) Loss measurements of the p- and s-wave Feshbach resonances of $|9/2,-7/2\rangle \otimes |9/2,-9/2\rangle$ as a function of the magnetic field for red laser detuning. The laser beam propagating along the $\hat{y}$ axis is linearly polarized parallel to the external magnetic field and red detuned by 1.1 GHz.

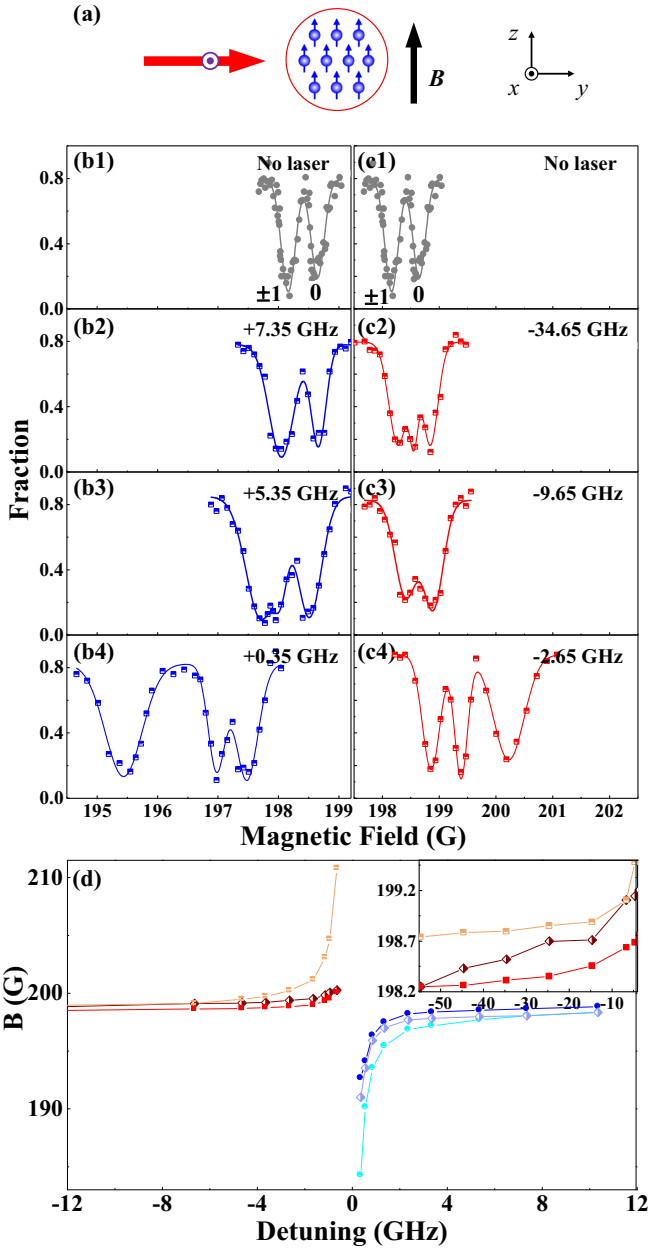

FIG. 5. The p-wave Feshbach resonance manipulated by the laser field with the polarization perpendicular to external magnetic field. (a) Schematic diagram of the laser beam and the external magnetic field. The laser beam propagating along the $\hat{y}$ axis is linearly polarized perpendicular to the external magnetic field. (b),(c) Atom-loss measurements of the p-wave Feshbach resonance of $|9/2,-7/2\rangle \otimes |9/2,-7/2\rangle$ as a function of the magnetic field for the different blue and red laser detuning. (d) The resonance position of the shifted Feshbach resonance as a function of the laser detuning. Three different lines correspond to the $m = 0$ and $m = \pm1$ resonances, respectively.

198.3 and 198.8 G are still some distance away from the s-wave resonance sitting at 202.1 G [41].

With our optical control, as shown in Fig. 4, for a red detuning of 1.1 GHz, one of the resonances with $m = 0$ can be shifted to the position very close to the s-wave resonance, which has also been shifted a few Gauss by the laser. Figure 4(a) shows the loss for a single-component Fermi gas with only the $|9/2, -7/2\rangle$ state and with applied optical control, and Fig. 4(b) shows the loss feature for a mixture of $|9/2, -7/2\rangle$ and $|9/2, -9/2\rangle$ with the same laser present. One can see that one of the p-wave resonances is entirely buried inside the s-wave resonance. In fact, by tuning the laser detuning, one has the flexibility of controlling the relative position between the p-wave and the s-wave resonances. Therefore, it creates the situation where the predications from Refs. [37–40] can be tested in this system.

VI. SHIFT INDUCED BY σ-POLARIZED LASER BEAM

We also consider the situation where the laser polarization is perpendicular to the magnetic field. In Fig. 5, we show the case where the laser propagates along $\hat{y}$, while the polarization is along $\hat{x}$. In this case, the laser breaks rotational symmetry along $\hat{z}$ and the $m = \pm 1$ resonances split as a result. We find that when the laser is red detuned and large in strength, one of the peaks from the $m = \pm 1$ manifold moves closer to the $m = 0$ resonance and they become incidentally degenerate, as shown in Fig. 5(c3). When the laser frequency is tuned further to the resonance, the $m = 0$ peak moves much more quickly, still consistent with the analysis in the previous part.

In Fig. 6, we show a different case in which the laser propagates along the magnetic field direction, but the polarization is circularly (or linearly) polarized in the plane perpendicular to the magnetic field (i.e., the xy plane). Here, we fix the laser detuning at -2.6 GHz and find that the resonance position behaves differently depending on the laser ellipticity ξ ($\xi = 0$ denote linear polarization, and $\xi = \pm 1$ denotes $\sigma_{\pm}$ polarization.) Thus, we see that by combining laser detuning and ellipticity, one can almost independently control all three resonances.

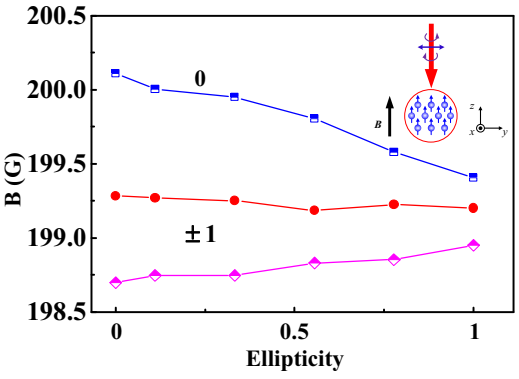

FIG. 6. The p-wave Feshbach resonance manipulated by the laser field propagating along the external magnetic field with circular polarization. The position of the shifted Feshbach resonance as a function of the ellipticity. Here, laser detuning is -2.6 GHz. Inset: Schematic diagram of the laser beam and the external magnetic field. Three different lines correspond to the $m = 0$ and $m = \pm 1$ resonances, respectively.

VII. CONCLUSION

In summary, we have studied the optical control of a p-wave Feshbach resonance by utilizing bound-to-bound transitions driven by a laser field. The main finding is a universal feature of this optical control, that is, the ratio $I(0)/I(\pm 1)$ to large extent is a universal constant. By this optical control, we demonstrate that intriguing scenarios can happen such as a p-wave resonance overlapping with an s-wave resonance. We have also considered the situation that the polarization of the laser is not along $\hat{z}$, but in the xy plane. This breaks the rotational symmetry and all three resonances will split. This allows us to access independent control of all three resonances. Our work opens many opportunities for investigating interesting few- and many-body problems in these settings.

ACKNOWLEDGMENTS

This work is supported by National Key R&D Program of China (Grants No. 2016YFA0301600 and No. 2016YFA0301602), NSFC Grants No. 11234008, No. 11474188, No. 11704234, No. 11325418, No. 11734010, No. 11434011, and No. 11674393, the Fund for Shanxi "1331 Project" Key Subjects Construction, the Fundamental Research Funds for the Central Universities, and the Research Funds of Renmin University of China under Grants No. 16XNLQ03 and No. 17XNH054.

P.P. and R.Z. contributed equally to this work.

APPENDIX: PROOF OF EQS. (3) AND (4)

Now we prove Eqs. (3) and (4) in the main text by calculate the intensity $I(m)$ of the laser-induced coupling between the closed-channel bound state and the excited molecular state.

We start with a brief introduction of the wave function of the molecular state $|l,m,\lambda,n_n,\{n_e\}\rangle$. Since the freedom of the inner-shell electron can be safely ignored, a homonuclear diatomic molecule, e.g., a molecule of two ^{40}K atoms, can

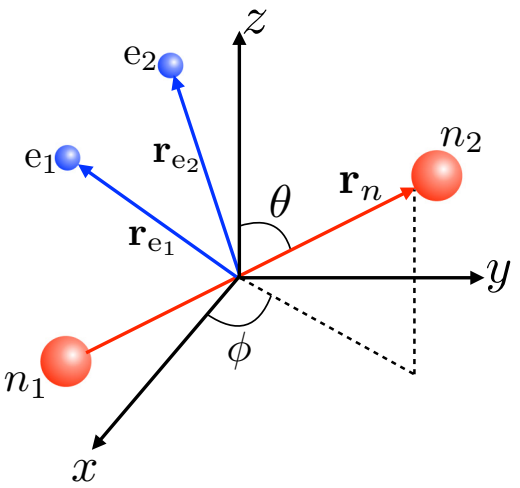

FIG. 7. The coordinate system used in our calculation.

be viewed as being composed of two nuclei $n_{1,2}$ and two outermost-shell electrons $e_{1,2}$ (Fig. 7). We study the relative motion of these four particles, which is decoupled from the center-of-mass motion. Thus, as shown in Fig. 7, we choose the origin of our coordinate system to be the center-of-mass position, which is approximated as the middle point of the two nuclei. We also define the x, y, and z axes to be parallel to the ones of the laboratory frame. In our system, the molecule wave function is a function of the relative position $\mathbf{r}_n$ of the two nuclei and the position $\mathbf{r}_{e_{1,2}}$ of the electrons $e_{1,2}$ (Fig. 7). Notice that $\mathbf{r}_{e_i}(i=1,2)$ is actually the relative position of e_i and the center of mass of the two nuclei. As shown in the main text, spin-orbit coupling and hyperfine interaction are ignored. Thus, in our calculation, we only consider the spatial motion of the electrons and nuclei.

In our system, the total orbital angular momentum of all four particles is denoted by $\mathbf{L}$, and the orbital angular momentum of the electron e_i $(i=1,2)$ is denoted by $\mathbf{L}_{e_i}$. For simplicity, we ignore the fine and hyperfine interaction and only consider the Coulomb interaction. Therefore, for our system, the total angular momentum $\mathbf{L}$ and the component of $\mathbf{L}_{e_1}+\mathbf{L}_{e_2}$ in the direction of $\mathbf{r}_n$ are conserved. Thus, the molecule state can be denoted as $|l,m,\lambda,n_n,\{n_e\}\rangle$, where l and m are the quantum numbers for $\mathbf{L}^2$ and the z component of $\mathbf{L}$, respectively, λ is the quantum number for the component of $\mathbf{L}_{e_1}+\mathbf{L}_{e_2}$ along the direction of $\mathbf{r}_n$, while n_n and $\{n_e\}$ are the nuclear and the electronic vibrational quantum numbers, respectively. Under the Born adiabatic approximation [42], the molecular wave function

$$\Psi_{l,m,\lambda,n_n,\{n_e\}}(\mathbf{r}_n;\mathbf{r}_{e_1},\mathbf{r}_{e_2}) \equiv \langle \mathbf{r}_n;\mathbf{r}_{e_1},\mathbf{r}_{e_2}|l,m,\lambda,n_n,\{n_e\}\rangle \quad \text{(A1)}$$

can be factorized as

$$\Psi_{l,m,\lambda,n_n,\{n_e\}}(\mathbf{r}_n;\mathbf{r}_{e_1},\mathbf{r}_{e_2}) = \psi^{(n)}_{l,m,\lambda,n_n,\{n_e\}}(\mathbf{r}_n)\psi^{(e)}_{\{n_e\},\lambda}(\mathbf{r}_n;\mathbf{r}_{e_1},\mathbf{r}_{e_2}). \quad \text{(A2)}$$

Here, $\psi^{(e)}_{\{n_e\},\lambda}$ is the wave function of the two outermost-shell electrons when the positions of the two nuclei are pinned down, and can be expressed as

$$\psi^{(e)}_{\{n_e\},\lambda}(\mathbf{r}_n;\mathbf{r}_{e_1},\mathbf{r}_{e_2}) = e^{-i\hat{L}^{(e)}_z\phi}e^{-i\hat{L}^{(e)}_y\theta}\phi_{\{n_e\},\lambda}(r_n;\mathbf{r}_{e_1},\mathbf{r}_{e_2}), \quad \text{(A3)}$$

where r_n, θ, and ϕ are the norm, polar angle, and azimuthal angle of $\mathbf{r}_n$, respectively (Fig. 7), $\hat{L}^{(e)}_\alpha$ $(\alpha=x,y,z)$ is the component of $\mathbf{L}_{e_1}+\mathbf{L}_{e_2}$ along the α axis, and $\phi_{\{n_e\},\lambda}$ is the electronic wave function when the nuclei are pinned on the z axis, which satisfies $\hat{L}^{(e)}_z\phi_{\{n_e\},\lambda}(r_n;\mathbf{r}_{e_1},\mathbf{r}_{e_2}) = \lambda\phi_{\{n_e\},\lambda}(r_n;\mathbf{r}_{e_1},\mathbf{r}_{e_2})$. Moreover, it can be shown that the nuclear wave function $\psi_{l,m,\lambda,n_n,\{n_e\}}(\mathbf{r}_n)$ can be further factorized as [43]

$$\psi_{l,m,\lambda,n_n,\{n_e\}}(\mathbf{r}_n) = \chi_{l,m,\lambda,n_n,\{n_e\}}(r_n) \times \sqrt{\frac{2l+1}{4\pi}}D^{(l)}_{\lambda,m}(\phi,\theta,0), \quad \text{(A4)}$$

with $D^{(l)}_{\lambda,m}(\alpha,\beta,\gamma)$ being the Wigner's D function and $\chi_{l,m,\lambda,n_n,\{n_e\}}(r_n)$ being the radial wave function of the nuclei. With the above results, we can calculate the dipole transition matrix element $\langle l^f,m,\lambda^f,n^f_n,\{n^f_e\}|\hat{T}_0|l^i,m,\lambda^i,n^i_n,\{n^i_e\}\rangle$, which appears in Eq. (2). This matrix element can be expressed as

$$\begin{aligned}&\langle l^f,m,\lambda^f,n^f_n,\{n^f_e\}|\hat{T}_0|l^i,m,\lambda^i,n^i_n,\{n^i_e\}\rangle \\ &= \int d\mathbf{r}_{e_1}d\mathbf{r}_{e_2}d\mathbf{r}_n\big[\Psi^*_{l^f,m,\lambda^f,n^f_n,\{n^f_e\}}(\mathbf{r}_n;\mathbf{r}_{e_1},\mathbf{r}_{e_2})\hat{T}_0 \\ &\times \Psi_{l^i,m,\lambda^i,n^i_n,\{n^i_e\}}(\mathbf{r}_n;\mathbf{r}_{e_1},\mathbf{r}_{e_2})\big], \end{aligned} \quad \text{(A5)}$$

where

$$\hat{T}_0 = (z_{e_1}+z_{e_2}), \quad \text{(A6)}$$

with z_{e_i} $(i=1,2)$ the z component of $\mathbf{r}_{e_i}$. For future use, we further define the operators

$$\hat{T}_{\pm1} = \left[\frac{\mp(x_{e_1}+x_{e_2})-i(y_{e_1}+y_{e_2})}{\sqrt{2}}\right], \quad \text{(A7)}$$

with x_{e_i} and y_{e_i} $(i=1,2)$ being the x and y component of $\mathbf{r}_{e_i}$, respectively. It is clear that $\hat{T}_j$ $(j=0,\pm1)$ form rank-1 irreducible tensor operators under the total rotation of the two electrons, and thus satisfy

$$e^{i\hat{L}^{(e)}_y\theta}e^{i\hat{L}^{(e)}_z\phi}\hat{T}_0e^{-i\hat{L}^{(e)}_z\phi}e^{-i\hat{L}^{(e)}_y\theta} = \sum_{q'=0,\pm1}\hat{T}_{q'}D^{(1)}_{q',0}(\phi,\theta,0). \quad \text{(A8)}$$

Substituting Eqs. (A3) and (A4) into Eq. (A2) and then into Eq. (A5), and using Eq. (A8) and the facts that $l^i=1$ and $\lambda^i=0$, we obtain

$$\begin{aligned}&\langle l^f,m,\lambda^f,n^f_n,\{n^f_e\}|\hat{T}_0|l^i,m,\lambda^i,n^i_n,\{n^i_e\}\rangle \\ &= (-1)^{\lambda^f-m}\sqrt{3(2l^f+1)}A_{\{n^f_e\},n^f_n,\{n^i_e\},n^i_n,l^f,m,\lambda^f} \\ &\times \begin{pmatrix} l^f & 1 & 1\\ -\lambda^f & \lambda^f & 0\end{pmatrix}\begin{pmatrix} l^f & 1 & 1\\ -m & 0 & m\end{pmatrix}, \end{aligned} \quad \text{(A9)}$$

where $\begin{pmatrix} j_1 & j_2 & j_3\\ m_1 & m_2 & m_3\end{pmatrix}$ is the Winger-3j symbols and $A_{\{n^f_e\},n^f_n,l^f,m,\lambda^f}$ is defined as

$$\begin{aligned}&A_{\{n^f_e\},n^f_n,\{n^i_e\},n^i_n,l^f,m,\lambda^f} \\ &= \int_0^\infty dr_n\left\{r_n^2\chi^*_{l^f,m,\lambda^f,\{n^f_e\},n^f_n}(r_n)\chi_{l^i=1,m,\lambda^i=0,\{n^i_e\},n^i_n}(r_n)\right. \\ &\left.\times\int d\mathbf{r}_{e_1}d\mathbf{r}_{e_2}\big[\phi^*_{\{n^f_e\},\lambda^f}(r_n;\mathbf{r}_{e_1},\mathbf{r}_{e_2})\hat{T}_{\lambda^f}\phi_{\{n^i_e\},\lambda^i=0}(r_n;\mathbf{r}_{e_1},\mathbf{r}_{e_2})\big]\right\}. \end{aligned} \quad \text{(A10)}$$

In the derivation of Eq. (A9), the relations that $D^{(l)}_{m'm}(\phi,\theta,0)^* = (-1)^{m'-m}D^{(l)}_{-m',-m}(\phi,\theta,0)$ and

$$\begin{aligned}&\int\frac{\sin\phi d\phi d\theta}{4\pi}D^{(j_1)}_{m'_1m_1}(\phi,\theta,0)D^{(j_2)}_{m'_2m_2}(\phi,\theta,0)D^{(j_3)}_{m'_3m_3}(\phi,\theta,0) \\ &= \begin{pmatrix} j_1 & j_2 & j_3\\ m'_1 & m'_2 & m'_3\end{pmatrix}\begin{pmatrix} j_1 & j_2 & j_3\\ m_1 & m_2 & m_3\end{pmatrix} \end{aligned} \quad \text{(A11)}$$

are adopted [43]. Now we consider the dependence of $A_{\{n^f_e\},n^f_n,\{n^i_e\},n^i_n,l^f,m,\lambda^f}$ on the quantum numbers l^f and m of the final state. In the radial Schrödinger equation satisfied by $\chi_{\{n^f_e\},n^f_n,l^f,m,\lambda^f}(r_n)$, the value of l^f and m only influence the intensity of the centrifugal potential which is proportional to $-r_n^{-2}$, and thus do not have strong effects for the deep bound state. As shown in the main text, here we assume that the excited molecular states are deep bound states and thus assume

the radial wave function $\chi_{\{n_e^f\},n_n^f,l^f,m,\lambda^f}(r_n)$ to be approximately independent of the values of l' and m. Therefore, according to Eq. (A10), the parameter $A_{\{n_e^f\},n_n^f,\{n_e^i\},n_n^i,l^f,m,\lambda^f}$ is also independent of l^f and m. Therefore, we can simplify the notation

$$A_{\{n_e^f\},n_n^f,\{n_e^i\},n_n^i,l^f,m,\lambda^f} \to A_{\{n_e^f\},n_n^f,\{n_e^i\},n_n^i,\lambda^f}, \tag{A12}$$

and rewrite Eq. (A9) in a more concise form as

$$\begin{aligned}&\langle l^f,m,\lambda^f,n_n^f,\{n_e^f\}|\hat{T}_0|l^i,m,\lambda^i,n_n^i,\{n_e^i\}\rangle \\ &= (-1)^{\lambda^f-m}\sqrt{3(2l^f+1)}A_{\{n_e^f\},n_n^f,\{n_e^i\},n_n^i,\lambda^f} \\ &\times \begin{pmatrix} l^f & 1 & 1 \\ -\lambda^f & \lambda^f & 0 \end{pmatrix}\begin{pmatrix} l^f & 1 & 1 \\ -m & 0 & m \end{pmatrix}.\end{aligned} \tag{A13}$$

Equation (A13) shows that the dependences of $\langle l^f,m,\lambda^f,\{n_e^f\},n_n^f|\hat{T}_0|l^i,m,\lambda^i,\{n_e^i\},n_n^i\rangle$ on l^f and m are all included in the Winger-3 j symbols and the factor $\sqrt{3(2l^f+1)}$, and thus can be evaluated precisely. Substituting Eq. (A13) into Eq. (2), we immediately obtain the laser coupling intensity $I(m)$:

$$I(m) = g(m,\lambda^f)h\left(\{n_e^f\},n_n^f,\{n_e^i\},n_n^i,\lambda^f\right), \tag{A14}$$

where

$$\begin{aligned}g(m,\lambda^f) = \sum_{l^f} 3(2l^f+1)&\begin{pmatrix} l^f & 1 & 1 \\ -\lambda^f & \lambda^f & 0 \end{pmatrix}^2 \\ &\times\begin{pmatrix} l^f & 1 & 1 \\ -m & 0 & m \end{pmatrix}^2,\end{aligned} \tag{A15}$$

and

$$h\left(\{n_e^f\},n_n^f,\{n_e^i\},n_n^i,\lambda^f\right) = \left|A_{\{n_e^f\},n_n^f,\{n_e^i\},n_n^i,\lambda^f}\right|^2. \tag{A16}$$

Equation (A14) is simply Eq. (3).

Furthermore, using Eqs. (A14)–(A16), we can immediately obtain the result $I(+1) = I(-1)$, as well as Eq. (4). Notice that this result is independent of the value of $\{n_e^f\}$. This result means that if the π-polarized laser couples the closed-channel bound state of the magnetic Feshbach resonance to the excited molecular states with $\lambda^f = 0$ (i.e., the states in the electronic Σ orbit), then the shift of the resonance point for $m = 0$ is more significant than that for $m = \pm 1$. On the other hand, if the excited molecular states have $\lambda^f = \pm 1$ (i.e., the states are in the electronic Π orbit), then the shift of the resonance point for $m = \pm 1$ is more significant than that for $m = 0$. This result implies that in all of our experiments, the laser induces the coupling to the excited molecule states with $\lambda^f = 0$.

[1] C. Chin, R. Grimm, P. Julienne, and E. Tiesinga, Rev. Mod. Phys. **82**, 1225 (2010).
[2] P. O. Fedichev, Yu. Kagan, G. V. Shlyapnikov, and J. T. M. Walraven, Phys. Rev. Lett. **77**, 2913 (1996).
[3] R. Yamazaki, S. Taie, S. Sugawa, and Y. Takahashi, Phys. Rev. Lett. **105**, 050405 (2010).
[4] R. Qi and H. Zhai, Phys. Rev. Lett. **106**, 163201 (2011).
[5] P. Zhang, P. Naidon, and M. Ueda, Phys. Rev. Lett. **103**, 133202 (2009).
[6] D. M. Bauer, M. Lettner, C. Vo, G. Rempe, and S. Dürr, Nat. Phys. **5**, 339 (2009).
[7] D. M. Bauer, M. Lettner, C. Vo, G. Rempe, and S. Dürr, Phys. Rev. A **79**, 062713 (2009).
[8] G. Thalhammer, M. Theis, K. Winkler, R. Grimm, and J. H. Denschlag, Phys. Rev. A **71**, 033403 (2005).
[9] H. Wu and J. E. Thomas, Phys. Rev. Lett. **108**, 010401 (2012).
[10] Z. Fu, P. Wang, L. Huang, Z. Meng, H. Hu, and J. Zhang, Phys. Rev. A **88**, 041601 (2013).
[11] L. W. Clark, L.-C. Ha, C.-Y. Xu, and C. Chin, Phys. Rev. Lett. **115**, 155301 (2015).
[12] A. Jagannathan, N. Arunkumar, J. A. Joseph, and J. E. Thomas, Phys. Rev. Lett. **116**, 075301 (2016).
[13] Y.-C. Zhang, W.-M. Liu, and H. Hu, Phys. Rev. A **90**, 052722 (2014).
[14] J. Jie and P. Zhang, Phys. Rev. A **95**, 060701 (2017).
[15] N. Read and D. Green, Phys. Rev. B **61**, 10267 (2000).
[16] T.-L. Ho and R. B. Diener, Phys. Rev. Lett. **94**, 090402 (2005).
[17] Z. Yu, J. H. Thywissen, and S. Zhang, Phys. Rev. Lett. **115**, 135304 (2015); **117**, 019901(E) (2016).
[18] S. M. Yoshida and M. Ueda, Phys. Rev. Lett. **115**, 135303 (2015).
[19] C. Luciuk, S. Trotzky, S. Smale, Z. Yu, S. Zhang, and J. H. Thywissen, Nat. Phys. **12**, 599 (2016).
[20] M. He, S. Zhang, H. M. Chan, and Q. Zhou, Phys. Rev. Lett. **116**, 045301 (2016).
[21] X. Cui, Phys. Rev. A **95**, 030701(R) (2017).
[22] A. Kitaev, Phys. Usp. **44**, 131 (2001)
[23] V. Gurarie, L. Radzihovsky, and A. V. Andreev, Phys. Rev. Lett. **94**, 230403 (2005).
[24] C.-H. Cheng and S.-K. Yip, Phys. Rev. Lett. **95**, 070404 (2005).
[25] C. A. Regal, C. Ticknor, J. L. Bohn, and D. S. Jin, Phys. Rev. Lett. **90**, 053201 (2003).
[26] C. Ticknor, C. A. Regal, D. S. Jin, and J. L. Bohn, Phys. Rev. A **69**, 042712 (2004).
[27] J. Zhang, E. G. M. van Kempen, T. Bourdel, L. Khaykovich, J. Cubizolles, F. Chevy, M. Teichmann, L. Tarruell, S. J. J. M. F. Kokkelmans, and C. Salomon, Phys. Rev. A **70**, 030702 (2004).
[28] K. Günter, T. Stöferle, H. Moritz, M. Köhl, and T. Esslinger, Phys. Rev. Lett. **95**, 230401 (2005).
[29] C. H. Schunck, M. W. Zwierlein, C. A. Stan, S. M. F. Raupach, W. Ketterle, A. Simoni, E. Tiesinga, C. J. Williams, and P. S. Julienne, Phys. Rev. A **71**, 045601 (2005).
[30] J. P. Gaebler, J. T. Stewart, J. L. Bohn, and D. S. Jin, Phys. Rev. Lett. **98**, 200403 (2007).
[31] J. Fuchs, C. Ticknor, P. Dyke, G. Veeravalli, E. Kuhnle, W. Rowlands, P. Hannaford, and C. J. Vale, Phys. Rev. A **77**, 053616 (2008).
[32] Y. Inada, M. Horikoshi, S. Nakajima, M. Kuwata-Gonokami, M. Ueda, and T. Mukaiyama, Phys. Rev. Lett. **101**, 100401 (2008).

[33] T. Nakasuji, J. Yoshida, and T. Mukaiyama, Phys. Rev. A **88**, 012710 (2013).
[34] A. Ludewig, *Feshbach Resonance in* ^{40}K (University of Amsterdam, 2012).
[35] P. Zhang, P. Naidon, and M. Ueda, Phys. Rev. A **82**, 062712 (2010).
[36] T. Köhler, K. Góral, and P. S. Julienne, Rev. Mod. Phys. **78**, 1311 (2006).
[37] L. Zhou, W. Yi, and X. Cui, Sci. China-Phys. Mech. Astron. **60**, 127011 (2017).
[38] F. Qin, X. Cui, and W. Yi, Phys. Rev. A **94**, 063616 (2016).
[39] L. Yang, X. Guan, and X. Cui, Phys. Rev. A **93**, 051605(R) (2016).
[40] Y. Jiang, D. V. Kurlov, X.-W. Guan, F. Schreck, and G. V. Shlyapnikov, Phys. Rev. A **94**, 011601(R) (2016).
[41] T. Loftus, C. A. Regal, C. Ticknor, J. L. Bohn, and D. S. Jin, Phys. Rev. Lett. **88**, 173201 (2002).
[42] J. Brown and A. Carrington, *Rotational Spectroscopy of Diatomic Molecules* (Cambridge University Press, Cambridge, 2003).
[43] L. D. Landau and E. M. Lifshitz, *Quantum Mechanics: Non-Relativistic Theory*, 3rd ed. (Pergamon, Oxford, 1977).